Inorg. Chem. **2003**, *42*, 6474–6483

Structural Insights into Aluminum Chlorofluoride (ACF)

Thoralf Krahl,[†] Reinhard Stösser,[†] Erhard Kemnitz,*[,†] Gudrun Scholz,[†] Michael Feist,[†] Gilles Silly,[‡] and Jean-Yves Buzaré[‡]

Institute of Chemistry, Humboldt University of Berlin, Berlin, Germany, and Laboratoire de l'Etat de Physique Condensé, UMR CNRS no. 6087, Université du Maine, Le Mans, France

Received January 31, 2003

The structure of the very strong solid Lewis acid aluminum chlorofluoride (ACF, $AlCl_xF_{3-x}$, $x = 0.05–0.3$) was studied by IR, ESR, Cl K XANES, ^{19}F MAS NMR, and ^{27}Al SATRAS NMR spectroscopic methods and compared with amorphous aluminum fluoride conventionally prepared by dehydration of α-$AlF_3 \cdot 3H_2O$. The thermal behavior of both compounds was investigated by DTA and XRD. In comparison to ACF, amorphous AlF_3 prepared in a conventional way is not catalytically active for the isomerization reaction of 1,2-dibromohexafluoropropane, which requires a very strong Lewis acid. Both compounds are mainly built up of corner-sharing AlF_6 octahedra forming a random network. The degree of disorder in ACF is higher than in amorphous AlF_3. Terminal fluorine atoms were detected in ACF by ^{19}F NMR. The chlorine in ACF does not exist as a separate, crystalline $AlCl_3$ phase. Additionally, chlorine-containing radicals, remaining from the synthesis, are trapped in cavities of ACF. These radicals are stable at room temperature but do not take part in the catalytic reaction.

1. Introduction

Aluminum chlorofluoride (ACF: $AlCl_xF_{3-x}$, $x = 0.05-0.30$) was developed in 1992 by DuPont.[1] It is a noncrystalline material which is formed during treatment of $AlCl_3$ with chlorofluorocarbons, such as $CFCl_3$, according to the equation

$$AlCl_3 + (3-x)CFCl_3 \rightarrow AlCl_xF_{3-x} + (3-x)CCl_4$$

ACF behaves like a very strong Lewis acid; it catalyzes the same reactions as antimony pentafluoride, and in some cases, it acts as an even stronger Lewis acid than the latter one.[2−6] Like all strong Lewis acids, it is moisture sensitive and must be stored under dry inert gas.

Another noncrystalline phase of AlF_3 (am-AlF_3) is known to emerge during heating of α-$AlF_3 \cdot 3H_2O$ to 200 °C under a self-generating atmosphere.[7] Although the overall composition of ACF and am-AlF_3 is similar, high Lewis acidity has not been observed for the latter. Therefore, the study of the differences between am-AlF_3 and ACF is of interest.

Despite known preparation routes for ACF and the testing of ACF for many catalytic reactions, only very little is known and understood about its physical and chemical nature. It is well-known from heterogeneous catalysis that the physical, the chemical, and especially the catalytic properties of a material are determined by the chemical nature of the components, by their inner and outer surface areas, and by the degree of disorder of the material. These aspects have not been considered in connection with ACF until now. It is therefore the aim of the present work to show that the combined action of those effects will be regarded as the main reason for the outstanding physical and chemical properties of ACF.

The samples investigated here are aluminum chlorofluoride (ACF), amorphous aluminum fluoride (am-AlF_3), and partially fluorinated aluminum chloride ($AlCl_xF_{3-x}$ with $x = 0.3-3.0$). The latter were investigated to determine the influence of the chlorine content on the properties of ACF. The samples were synthesized, characterized, and compared with the crystalline phases α- and β-AlF_3. Since most of the

* To whom correspondence should be addressed. E-mail: Erhard=Kemnitz@chemie.hu.berlin.de.
† Humboldt University of Berlin.
‡ Université du Maine.

(1) Sievert, A. C.; Krespan, C. G.; Weigert, F. J. (DuPont Co.) U.S. Patent 5,157,171, 1992.
(2) Krespan, G. C.; Petrov, V. A. *Chem. Rev.* **1996**, *96*, 3269−3301.
(3) Krespan, G. C.; Dixon, D. A. *J. Fluorine Chem.* **1996**, *77*, 117−126.
(4) Petrov, V. A.; Krespan, G. C.; Smart, B. E. *J. Fluorine Chem.* **1996**, *77*, 139−142.
(5) Petrov, V. A.; Krespan, G. C.; Smart, B. E. *J. Fluorine Chem.* **1998**, *89*, 125−130.
(6) Petrov, V. A.; Krespan, G. C. *J. Fluorine Chem.* **2000**, *102*, 199−204.
(7) Scholz, G.; Stösser, R.; Sebastian, S.; Kemnitz, E.; Bartoll, J. *J. Phys. Chem. Solids* **1999**, *60*, 153−162.

10.1021/ic034106h CCC: $25.00
Published on Web 09/03/2003

samples studied are noncrystalline, methods other than X-ray diffraction had to be used for structural characterization. Hence, the samples were investigated by IR and ESR spectroscopy, ^{19}F and ^{27}Al MAS NMR, and X-ray absorption spectra of the Cl K edge for the chlorine-containing species. The BET surface area of ACF, the average pore sizes, and the pore volumes were also determined.

There is also special interest in the crystallization behavior of ACF and am-AlF_3. The thermal behavior was studied by DTA followed by X-ray diffraction of the bulk phase. In addition, organic compounds evolved during heating were determined by gas-phase IR spectroscopy.

2. Experimental Section

2.1 Methods. X-ray diffraction (XRD) measurements were performed on a Seiffert RD7 (Freiberg, Germany) with Cu Kα radiation. Moisture sensitive samples were prepared in a drybox, covered with a special X-ray amorphous polystyrene foil, and sealed with Kel-F grease (Roth, Germany). Phases were identified by comparison with the ICSD powder diffraction file.[8]

FT-IR spectra of CsI pellets were recorded on a Perkin-Elmer 2000 spectrometer in transmission mode. About 250 mg of CsI (for optical properties, Fluka, Germany) was pressed with 1.5−2.0 mg of the sample inside the drybox, and then the samples were measured in the regions 4000−400 and 700−200 cm^{-1}. The gas phase spectra were measured using a 10 cm long Teflon cell equipped with KBr windows.

Specific BET surface areas[9] and pore size distributions were determined by low temperature nitrogen adsorption using a Micromeritics ASAP 2000. Samples were degassed in a vacuum at 200 °C before measurement.

The ESR measurements were carried out on a spectrometer ERS 300 (X-band (9 GHz), ZWG Berlin-Adlershof, Germany). For the data acquisition as well as computer control of the spectrometer, the control unit of the Magnettech Co. (Germany) was used. The spectra were simulated using the programs COMPAR[10] and ESR-MAKRO.[11] Spectra were recorded at room temperature, if not mentioned otherwise.

Solid state NMR experiments were done on a Bruker AVANCE 300 spectrometer using a 2.5 mm double-bearing magic angle spinning (MAS) probe with a decoupling channel optimized for ^{19}F observation. The samples were characterized at room temperature by measurements of ^{19}F ($I = {}^1/_2$, 282.4 MHz) and ^{27}Al ($I = {}^5/_2$, 78.2 MHz) nuclei. ^{19}F MAS NMR was performed at a spinning speed of 35 kHz; the measured parameter was the isotropic chemical shift δ_{iso}. ^{27}Al MAS satellite transition spectroscopy (SATRAS) experiments were performed at two spinning rates, 25 and 3 kHz, as described in ref 12. The measured NMR parameters were the quadrupolar frequency $\nu_Q = 3eQV_{zz}/2I(2I - 1)h$, the asymmetry parameter $\eta_Q = (V_{xx} - V_{yy})/V_{zz}$, and the isotropic chemical shift δ_{iso}. Hexafluorobenzene[13] and an aqueous 1 M solution of aluminum nitrate were used as reference for the ^{19}F and ^{27}Al chemical shifts, respectively, at room temperature and are accurate to ±1 ppm.

The solution ^{19}F NMR spectra were recorded on a Bruker DPX 300 spectrometer in $CDCl_3$ with an internal standard of C_6F_6[13] (set to 0 ppm) at a resonance frequency of 282.4 MHz.

Measurements of X-ray absorption spectra were carried out at HASYLAB on the beamline E4 (DESY, Hamburg, Germany) in transmission mode. The edge energy of the Cl K shell was 2822.0 eV; photon energies are accurate to ±0.2 eV. Samples were prepared in a drybox.

Table 1. Catalytic Activity in the Isomerization of 1,2-Dibromohexafluoropropane and Molar $AlCl_3$ Content of the Investigated Compounds Extracted from the Simulation of the ^{27}Al MAS SATRAS NMR Spectra

compd	catalytic activity [%]	$AlCl_3$ content [%]
$AlCl_3$	<0.1	100
$AlCl_{2.39}F_{0.61}$	0.1	85
$AlCl_{1.75}F_{1.25}$	9.3	66
$AlCl_{1.25}F_{1.75}$	20.7	24
$AlCl_{0.80}F_{2.20}$	41.6	21
ACF-013 $AlCl_{0.13}F_{2.87}$	>90.0	0
am-AlF_3	inactive	

2.2 Sample Preparation. If not mentioned otherwise, all preparations were consequently carried out under standard Schlenk conditions. Solvents were dried before using and stored over molecular sieves. Abbreviations for the samples used in this study are given in Table 1.

Aluminum Chlorofluoride (ACF-013). ACF was prepared from aluminum chloride (99.99%, Aldrich) containing 10 ppm Fe. About 10−20 g of $AlCl_3$ was filled into a round-bottomed flask equipped with a dry ice condenser. The flask was cooled with ice. $CFCl_3$ (5 equiv, 99.5%, Fluka, Germany) was added slowly over 15 min. The suspension was stirred at 0 °C for 1 h and then for 3 h at room temperature. The heat of the reaction refluxed the solvent (bp 23.8 °C) without further heating. After removing the solvent in a vacuum, quantitative amounts of the fine yellow powder ACF were obtained and stored in the glovebox. The sample used for investigation here correlated with the formula $AlCl_{0.13}F_{2.87}$ and contained 0.44 wt % carbon. This sample will be referred to as ACF-013.

Samples with a lower fluorine content were synthesized using less $CFCl_3$. If less than 1.5 molar equiv was used, $AlCl_3$ was first suspended in perfluorohexane to obtain a stirrable liquid. The composition of each sample was determined by Cl and F analysis (see Table 1).

Noncrystalline AlF_3 (am-AlF_3). α-$AlF_3 \cdot 3H_2O$ was annealed at 200 °C in a special platinum Q-crucible under self-generated atmosphere (quasi-isobar conditions[14]) for 2 h. This sample is further named am-AlF_3 (see Table 1).

α-AlF_3. α-AlF_3 was prepared by thermal decomposition of α-NH_4AlF_4 in an open corundum crucible in flowing nitrogen by heating to 700 °C at 5 K/min and holding this temperature for 4 h. The phase purity was confirmed by XRD.[8]

***β*-AlF_3.** β-AlF_3 was prepared by thermal decomposition of α-$AlF_3 \cdot 3H_2O$ under self-generating atmosphere by heating to 400 °C at 5 K/min and holding this temperature for 2 h. The phase purity was confirmed by XRD.[8]

(8) Powder Diffraction File, ICPDS-ICDD 2001, PDF numbers used: 44-231 (α-AlF_3), 84-1672 (β-AlF_3), 47-1659 (θ-AlF_3), 43-436 (α-$AlF_3 \cdot 3H_2O$), 35-827 (β-$AlF_3 \cdot 3H_2O$), 76-56 (α-NH_4AlF_4), 22-10 ($AlCl_3$), 44-1473 ($AlCl_3 \cdot 6H_2O$), 41-380 (AlF_2OH, isomorphous with η-AlF_3).

(9) Brunauer, S.; Emmet, P. H.; Teller, E. *J. Am. Chem. Soc.* **1938**, *60*, 309−319.

(10) *Program COMPAR: Software of the Spectrometer ERS-300*; Zentrum für wissenschaftlichen Gerätebau: Berlin, 1990.

(11) Scholz, G.; Stösser, R.; Krossner, M.; Klein, J. *Appl. Magn. Reson.* **2001**, *21*, 105−123.

(12) Scholz, G.; Stösser, R.; Klein, J.; Silly, G.; Buzaré, J. Y.; Laligant, Y.; Ziemer, B. *J. Phys.: Condens. Matter* **2002**, *14*, 2101−2117.

(13) $\delta_F(C_6F_6)$ vs $CFCl_3$ −162.2 ppm.

(14) Menz, D. H.; Bentrup, U. *Z. Anorg. Allg. Chem.* **1989**, *576*, 186−196.

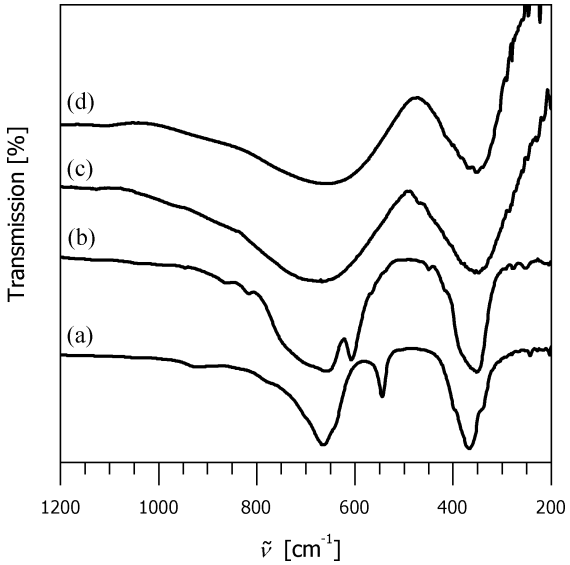

Figure 1. IR spectra of (a) α-AlF_3, (b) β-AlF_3, (c) ACF-013, and (d) am-AlF_3.

Irradiation of CCl_4. Tetrachloromethane was irradiated at 77 K with ultraviolet light of 254 nm wavelength inside a quartz dewar and then transferred together with liquid nitrogen into the dewar of the ESR cavity. This procedure was applied to avoid the spectral inference of E' centers formed in quartz by the short wavelength of UV radiation.

Test of Catalytic Activity. About 20 mg of the corresponding sample was filled into a 10 mL V-shaped flask and closed with a septum inside the glovebox. The 1,2-dibromohexafluoropropane (10 μL per mg sample, 99%, FluoroChem, U.K.) was added, and the suspension was stirred at room temperature for 2 h. After that the catalyst was hydrolyzed with water, the organic phase was investigated by ^{19}F NMR.[5] When the organic phase solidified during the reaction (more then 75% conversion), the flask was slightly heated during hydrolysis of the catalyst. The degree of conversion to 2,2-dibromohexafluoropropane (mp 52 °C) was determined by integration of the signals in the NMR spectrum. ^{19}F NMR (282 MHz, $CDCl_3$): reactant, δ 28.9 (m, 1F, C*F*Br), 87.9 (m, 3F, C*F*$_3$), 103.0 (dm, 1F, C*F*FBr, $^2J_{FF}$ = 176 Hz), 105.0 (dm, 1F, CF*F*Br, $^2J_{FF}$ = 176 Hz), ppm; product, δ 90.1 (s, C*F*$_3$) ppm.

3. Results

3.1 Spectroscopic Investigation of ACF and am-AlF_3. XRD, IR, Catalysis, and BET. ACF-013 and am-AlF_3 do not show any distinct reflections in the X-ray powder diffractograms, whereas the samples of fluorinated $AlCl_xF_{3-x}$ with x = 0.8−2.6 show more or less distinct reflections of $AlCl_3$.

The IR spectra of ACF-013 and am-AlF_3, and of the α-AlF_3 and β-AlF_3 crystalline phases, are given in Figure 1. Both α-AlF_3 and β-AlF_3 show two strong bands in regions of 660 and 350 cm^{-1}. These crystalline phases have additional, weaker bands at 607 and 544 cm^{-1}, respectively. The spectra of ACF-013 and am-AlF_3 differ somehow from the spectra of the crystalline phases. They show two very broad signals around 660 and 350 cm^{-1} without any further structuring. The spectra of partially fluorinated $AlCl_3$ samples can be interpreted as a superposition of those of $AlCl_3$ and ACF-013.

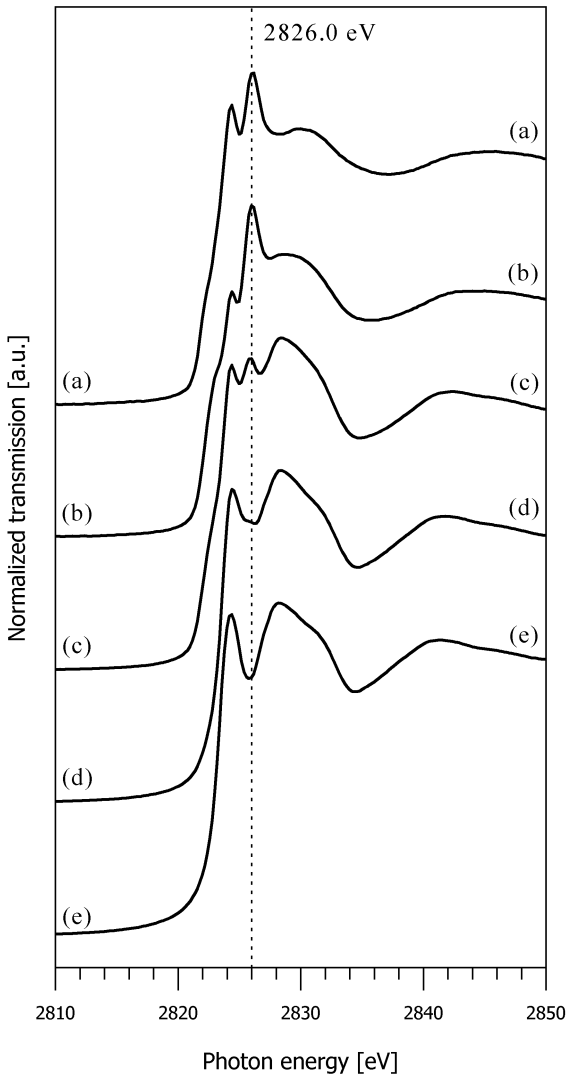

Figure 2. X-ray absorption spectra of the Cl K edge of (a) ACF-013, (b) $AlCl_{0.80}F_{2.20}$, (c) $AlCl_{1.75}F_{1.25}$, (d) $AlCl_{2.39}F_{0.61}$, and (e) $AlCl_3$.

The catalytic activity of ACF-013 for the isomerization of 1,2-dibromohexafluoropropane is high (80−90% conversion), whereas $AlCl_3$ has conversion rates below 0.1% under the conditions applied here. The samples of fluorinated $AlCl_3$ yield lower catalytic activities than ACF-013 (see Table 1). After being exposed to air for 1 day, ACF-013 is no longer catalytically active. As expected, am-AlF_3 is inactive in this reaction.

The specific BET surface area of ACF-013 is 101.1 ± 0.6 m^2/g. The total pore volume is 0.081 cm^3/g, and the average pore size is 31.9 Å. The BET surface area of am-AlF_3 could not be determined. No equilibrium could be achieved during low temperature N_2 adsorption, due to remaining water content. As observed before, the surface areas of the polycrystalline α- and β-AlF_3 are in the range of 40 m^2/g.[15]

XANES. Normalized X-ray absorption spectra of the Cl K edge (2822.0 eV) of $AlCl_3$, ACF-013, and partially fluorinated $AlCl_3$ are shown in Figure 2. None of the spectra

(15) Kemnitz, E.; Menz, D. H. *Prog. Solid State Chem.* **1998**, *26*, 97−153.

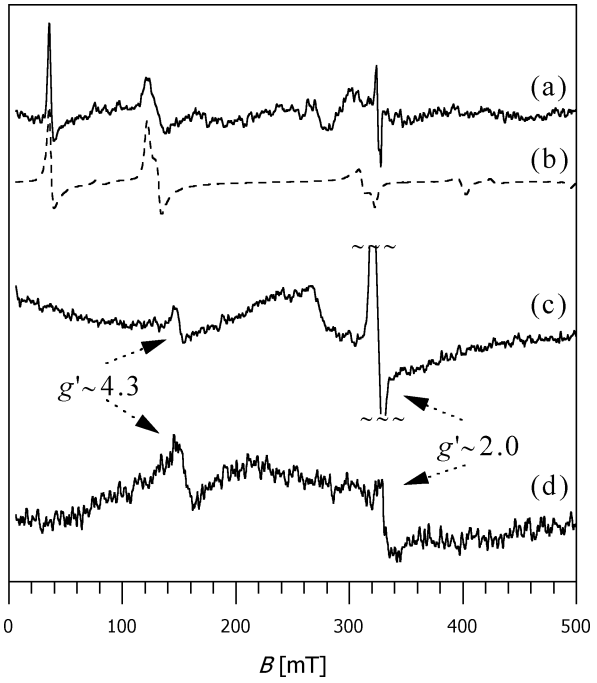

Figure 3. X-band ESR spectra: (a) experimental spectrum of $AlCl_3$, (b) simulated spectrum for $AlCl_3$:Fe^{3+} with the parameters $S = {}^5/_2$, $g = 2.0$, $D = -5670.0$ MHz, $E = 48.3$ MHz, $a = -6.6$ MHz, $F = -62.0$ MHz,[16] (c) experimental spectrum of ACF-013, the intensive signal at $g' \sim 2$ was discriminated, and (d) experimental spectrum of am-AlF_3.

shows a pre-edge absorption. $AlCl_3$ exhibits a sharp resonance at 2824.4 eV and a broader one at 2828.2 eV. During the process of fluorination, the resonance at 2824.4 eV loses intensity, and the broader resonance at 2828.2 eV also loses intensity and is shifted to higher energy values (2830.0 eV in ACF-013). With increasing fluorine content of the sample, a new characteristic and sharp resonance at 2826.0 eV appears. Spectra of samples with medium fluorine content can be recognized as a superposition of the spectra of $AlCl_3$ and ACF-013.

ESR. Aluminum chloride used in the preparation of ACF-013 has few signals in the X-band ESR spectrum originating essentially from Fe^{3+} ions (Figure 3a). This powder spectrum was simulated using the parameters obtained from single crystal measurements of Fe^{3+} in an $AlCl_3$ matrix[16] (Figure 3b). In addition, a symmetric signal of unknown origin appeared at $g' \sim 2$.

The ESR spectra of ACF-013 and am-AlF_3 recorded in X-band in the whole spectral range are shown in Figure 3c,d, respectively. They exhibit two broad resonances of low intensity at $g' \sim 4.3$ and $g' \sim 2.0$. ACF-013 has an additional, intensive signal at $g' \sim 2$.

The latter, measured at room temperature and 77 K, is shown magnified in Figure 4a,b, respectively. With increasing fluorine content, the signal gains in intensity, while simultaneously the components are resolved worse (compare Figure 4b,c). The resulting spectral pattern including the *g*-shift to higher values led to the tentative assignment of radicals derived from CCl_4. Since CCl_4 and its precursors

(16) Bang, G.; Sperlich, G.; Becker, W.-J. *Phys. Status Solidi* **1970**, *41*, 369−374.

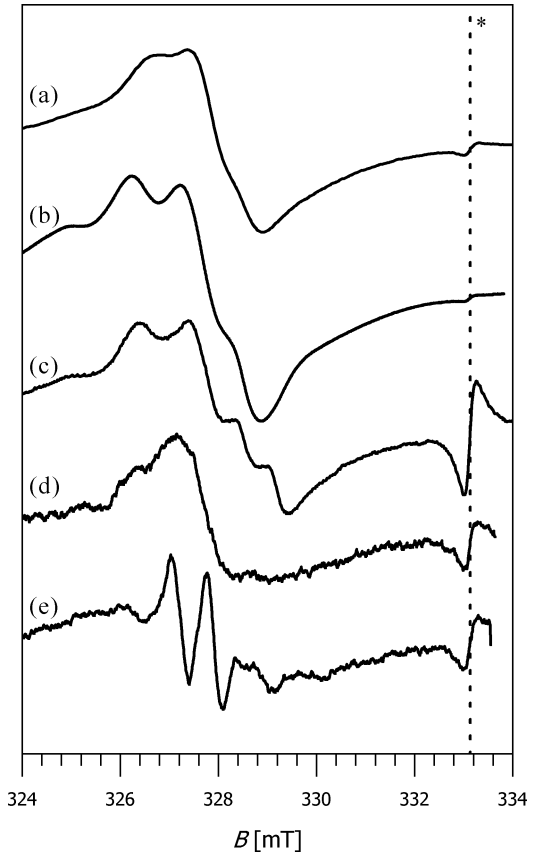

Figure 4. Experimental X-band ESR spectra of (a) ACF-013, 293 K, (b) ACF-013, 77 K, (c) $AlCl_{2.39}F_{0.61}$, 77 K, (d) irradiated CCl_4, 77 K, and (e) irradiated CCl_4, 220 K. Asterisk (*) indicates internal standard MgO:Cr^{3+}.

are involved in the synthesis of ACF-013, the formation of such radicals can be expected. For comparison, a corresponding radical was generated photochemically in a tetrachloromethane matrix (77 K, 254 nm), and its spectrum is presented in Figure 4d,e. Comparison of these spectra with that of ACF-013 shows the expected similarities between the systems, keeping in mind that in both cases a superposition of different chlorine containing radicals appeared.

It should be noted that the radical signal does not undergo changes while performing the isomerization reaction of 1,2-dibromohexafluoropropane inside the cavity of the ESR spectrometer.

^{19}F MAS NMR. The ^{19}F MAS NMR spectrum of ACF-013 is presented in Figure 5. Three types of components are evidenced corresponding to three different ranges of ^{19}F isotropic chemical shift δ_{iso} values. The main one (type 1) has a δ_{iso} value close to 0 ppm as in the various AlF_3 phases. The second contribution (type 2) is related to unusual negative δ_{iso} values of about −40 ppm. The third type consists of very small and narrow lines in the 50−100 ppm range, which corresponds to organic fluorine compounds.

Figure 5 shows the best reconstruction of the experimental spectrum with two lines for both the type 1 and type 2 components. The corresponding parameters are given in the Figure 5 caption. The deconvolution was achieved using the DMFIT program[17] assuming anisotropic chemical shifts and Gaussian line shapes. ^{19}F dipolar coupling was not explicitly taken into account.

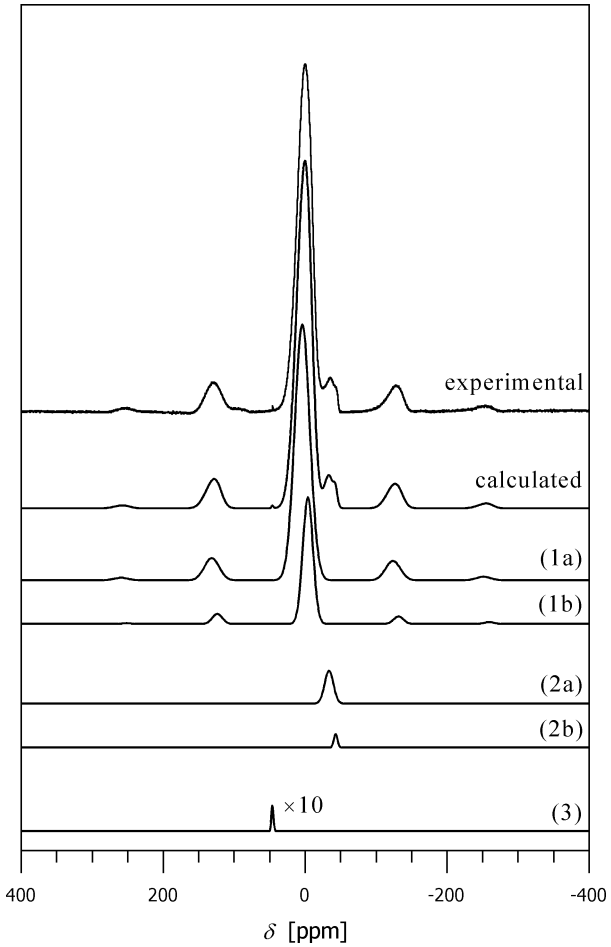

Figure 5. Experimental and calculated ^{19}F MAS NMR spectra (35 kHz spinning speed). The calculated spectrum is the sum of five components. Type 1 ^{19}F: (1a) $\delta_{iso} = 3.5$ ppm; width, 24 ppm; rel int, 71%; (1b) $\delta_{iso} = -4$ ppm; width, 16 ppm; rel int, 23%. Type 2 ^{19}F: (2a) $\delta_{iso} = -33$ ppm; width, 14 ppm; rel int, 5%; (2b) $\delta_{iso} = -42$ ppm; width, 6 ppm; rel int, 1%. Type 3 ^{19}F: (3) $\delta_{iso} = 44$ ppm; width, 3 ppm; rel int, ≈0%.

Samples of partially fluorinated $AlCl_3$ show very similar spectra. The relative intensities of the ^{19}F type 2 lines increase with higher fluorine content. This is shown by comparing the spectra of ACF-013 and $AlCl_{2.39}F_{0.61}$ (Figure 6a,c). The spectrum of am-AlF_3 is shown in Figure 6b. It exhibits only one line of type 1 with a δ_{iso} value of 2 ppm.

Experiments were also done on compounds which were hydrolyzed after exposure to air for 6 h, but which remained in a powder state afterward (ACF-013, $AlCl_{0.80}F_{2.20}$, and $AlCl_{1.25}F_{1.75}$). Only one intense signal of type 1 was observed in these spectra. Compared to ACF-013 and crystalline AlF_3, the lines are shifted to higher value by about 6 ppm (Figure 6d for ACF-13).

For comparison, ^{19}F NMR spectra recorded for various crystalline AlF_3 phases (α-AlF_3, β-AlF_3, α-$AlF_3{\cdot}3H_2O$, β-$AlF_3{\cdot}3H_2O$) are included in Figure 6. Note that δ_{iso} shifts toward higher values (about 20 ppm) from the pure AlF_3 phases to the corresponding hydrated ones.

^{27}Al Solid State NMR. ^{27}Al SATRAS NMR spectra of ACF-013 were recorded at 25 and 3 kHz spinning speeds.

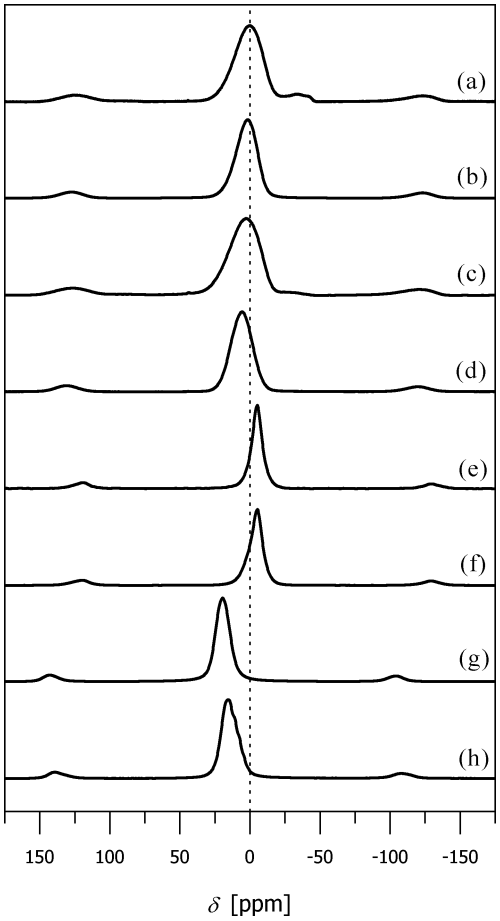

Figure 6. ^{19}F MAS NMR spectra recorded at 35 kHz for different phases of AlF_3: (a) ACF-013, (b) am-AlF_3, (c) $AlCl_{2.39}F_{0.61}$, (d) hydrolyzed ACF-013, (e) α-AlF_3, (f) β-AlF_3, (g) α-$AlF_3{\cdot}3H_2O$, and (h) β-$AlF_3{\cdot}3H_2O$.

The 25 kHz spectrum is presented in Figure 7. The shape of the central transition obtained for the highest speed (see insert) is characteristic of a disordered material with a distribution of quadrupolar frequencies.

We used the same theoretical treatment of the SATRAS NMR spectra[18−20] as in a previous study of nanostructured alumina.[12] Since the solid is amorphous, the spectra cannot be explained using single values for the quadrupolar parameters, ν_Q and η_Q. The broad envelope of the spinning sidebands of the satellite transition is reproduced well by simulation using a two-dimensional Czjzek distribution[12,21,22] $P(\nu_Q,\eta_Q)$

$$P_{d,\sigma}(\nu_Q, \eta_Q) = \frac{\nu_Q^{\,d-1}}{\sqrt{2\pi}\sigma^d}\eta_Q(1 - \eta_Q{}^2/9)\exp\left\{-\frac{\nu_Q^{\,2}}{2\sigma^2}(1 + \eta_Q{}^2/3)\right\}$$

with $d = 3$ and $\sigma = (440 \pm 40)$ kHz (Figure 7). The δ_{iso} parameter was -13 ± 1 ppm. The individual line width was assigned equal to 1.2 kHz. For a fine reconstruction of the

(17) Massiot, D.; Fayon, F.; Capron, M.; King, I.; Le Calvé, S.; Alonso, B.; Durand, J.-O.; Bujoli, B.; Gan, Z.; Hoatson, G. *Magn. Reson. Chem.* **2002**, *40*, 70−76.

(18) Skibsted, J.; Vosegaard, T.; Bildsoe, H.; Jakobsen, H. J. *J. Phys. Chem.* **1996**, *100*, 14872−14881.
(19) Skibsted, J.; Nielsen, N. C.; Bildsoe, H.; Jakobsen, H. J. *J. Magn. Reson.* **1991**, *95*, 88−117.
(20) Ding, S.; McDowell, C. A. *Chem. Phys. Lett.* **2001**, *333*, 413−418.
(21) Czjzek, G.; Fink, J.; Götz, F.; Schmidt, H.; Coey, J. M. D.; Rebouillat, J. P.; Lienard, A. *Phys. Rev. B* **1981**, *23*, 2513−2530.
(22) Czjzek, G. *Phys. Rev. B* **1982**, *25*, 4908−4910.

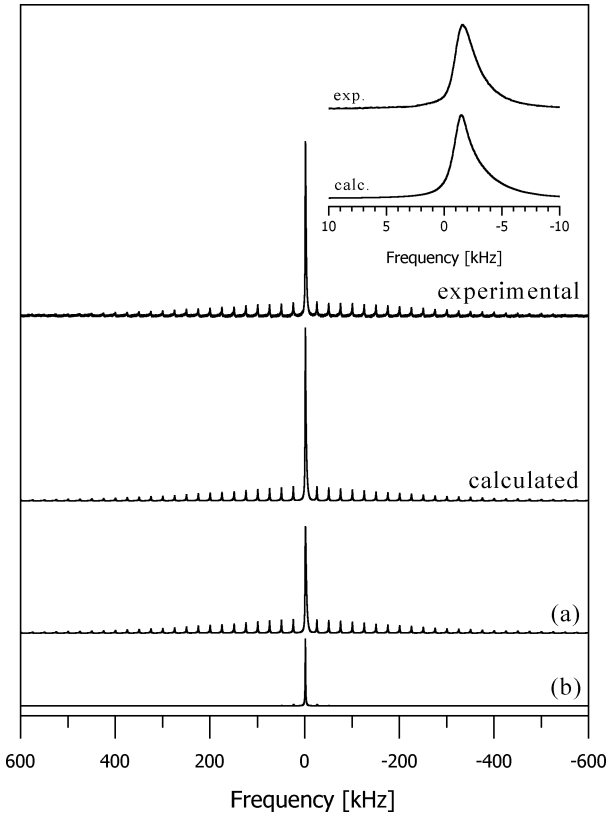

Figure 7. Experimental and calculated ^{27}Al MAS SATRAS NMR spectra (25 kHz spinning speed). The calculated spectrum is the sum of two components: (a) contribution calculated with a Czjzek distribution of quadrupolar parameters ($\sigma = 440$ kHz, $d = 3$); (b) contribution calculated with $\nu_Q = 11$ kHz. Details of the central line shown in the insert.

central transition, a second contribution evidenced on the 3 kHz spectrum with $\nu_Q = (11\pm2)$ kHz, $\eta_Q = 0.5\pm0.5$, and $\delta_{iso} = (-19\pm1)$ ppm with the same line width has to be taken into consideration. It corresponds to 10% of the Al nuclei.

In Figure 8, the ^{27}Al SATRAS NMR spectra of ACF-013 and am-AlF_3 measured at 25 kHz are compared. The latter exhibits a narrower central line and spinning sideband envelope. This is in agreement with the smaller Czjzek parameter $\sigma = (360 \pm 40)$ kHz deduced from the simulation of the spectrum. Both distributions are compared in Figure 9. The corresponding parameters in α-AlF_3 measured here are $\nu_Q = (32\pm4)$ kHz, $\eta_Q = 0$, and $\delta_{iso} = (-19\pm1)$ ppm.[23,24]

Samples of partially fluorinated $AlCl_3$ were also investigated at two spinning speeds. All the spectra recorded at 25 kHz give evidence of two main contributions: a crystalline one and a disordered one like ACF-013. The reconstruction of these spectra recorded at 3 kHz spinning speed demonstrated that the crystalline phase corresponds to a superposition of the main component with $\nu_Q = (65 \pm 5)$ kHz, $\eta_Q = 0.27 \pm 0.05$, $\delta_{iso} = (-2.5 \pm 1)$ ppm, and a line width equal to 0.3 kHz (crystalline $AlCl_3$ phase[25]) in addition to a small one (8%) with $\nu_Q = (8\pm2)$ kHz and the same isotropic chemical shift. The amount of crystalline $AlCl_3$ extracted from the simulation of the spectra at 25 kHz is given in Table 1 and Figure 10.

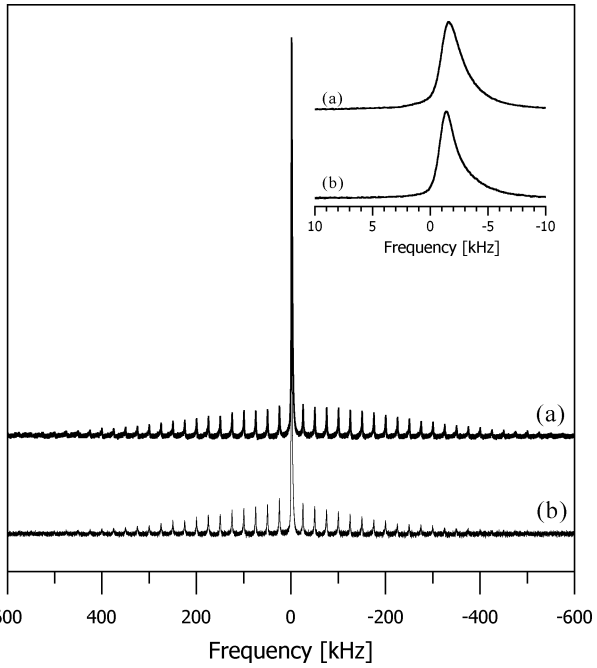

Figure 8. Experimental ^{27}Al MAS SATRAS NMR spectra (25 kHz spinning speed): (a) ACF-013 and (b) am-AlF_3. Details of the central line shown in the insert.

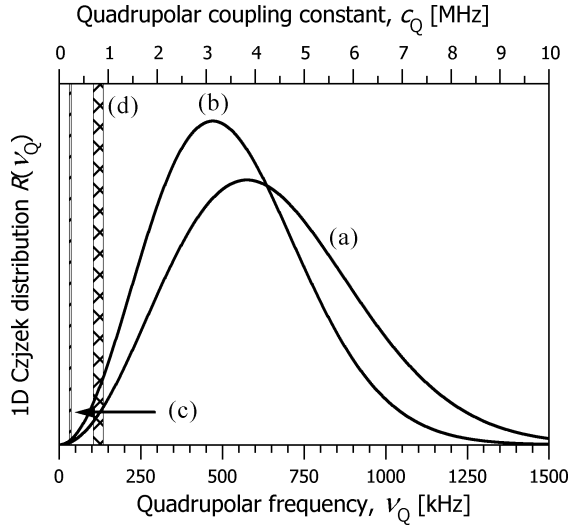

Figure 9. 1D Czjzek distributions $R(\nu_Q) = \int_0^1 P_{d,\sigma}(\nu_Q, \eta_Q)\, d\nu_Q$ with $d = 3$ for (a) ACF-013, $\sigma = 440$ kHz, and (b) am-AlF_3, $\sigma = 360$ kHz. For comparison, the quadrupolar frequencies including the error bars are shown for (c) α-AlF_3 and (d) β-AlF_3.[22] Note that $c_Q = 2/3\nu_Q I(2I - 1)$.

The spectra of the hydrolyzed compounds studied, $AlCl_{0.80}F_{2.20}$ and $AlCl_{1.25}F_{1.75}$, show that the $AlCl_3$ spectrum is reduced to a contribution with $\nu_Q = (4 \pm 2)$ kHz and $\delta_{iso} = (-2.5 \pm 1)$ ppm, whereas the ACF-013 part seems to remain almost unaffected.

3.2 Thermal Behavior of ACF and am-AlF3. Thermal analysis. The thermal behavior of ACF-013 was studied by DTA measurements in sealed quartz ampules. In order to distinguish between reversible and irreversible transitions, a temperature program including multiple heating and cooling runs and different maximum temperatures was applied.

(23) Chupas, P. J.; Ciraolo, M. F.; Hanson, J. C.; Grey, C. P. *J. Am. Chem. Soc.* **2001**, *123*, 1694−1702.
(24) Delattre, J. L.; Chupas, P. L.; Grey, C. P.; Stacy, A. M. *J. Am. Chem. Soc.* **2001**, *123*, 5364−5365.
(25) Ding, S.; McDowell, C. A. *J. Magn. Reson. A* **1995**, *112*, 36−42.

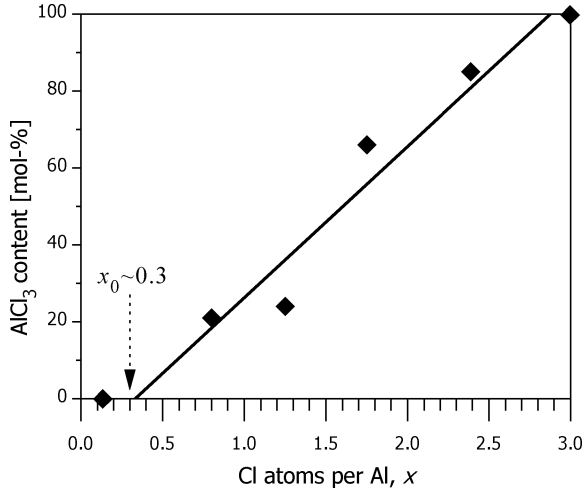

Figure 10. Molar $AlCl_3$ content of $AlCl_xF_{3-x}$ versus x from Table 1. The straight line corresponds to a linear regression for $x > 0.3$.

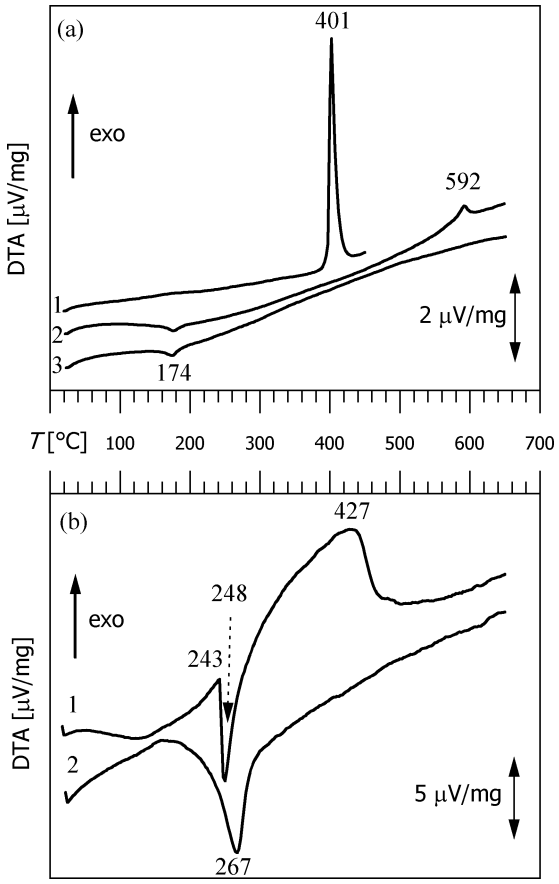

Figure 11. DTA measurements of (a) ACF-013 and (b) am-AlF_3 in quartz ampules. 1, 2, and 3 indicate the number of the heating cycle.

Figure 11a shows the heating curves for ACF-013. During the first heating, a sharp and intensive exothermic signal with an onset temperature of 400 °C and a peak temperature of 401 °C occurs, indicating an irreversible process. Therefore, the second heating shows thermal effects of a new phase composition characterized by a weak, reversible endothermic effect at 174 °C and an irreversible exothermic effect at 592 °C; the latter exclusively occurred during the second heating. Consequently, the third heating showed only the weak endothermic signal at 174 °C.

The X-ray diffractogram of the remaining phase recorded in an open sample holder showed β-AlF_3 and a small amount of $AlCl_3 \cdot 6H_2O$. The hydrate was formed by the uptake of water by $AlCl_3$ during the diffraction measurement.

The thermal behavior of am-AlF_3 is completely different from that of ACF-013. Its DTA curves are shown in Figure 11b. They exhibit a weak, broad endothermic region with a maximum at about 120 °C. It is followed by a sharp endothermic effect with an onset temperature of 243 °C and a peak temperature of 248 °C, and a broad exothermic peak with a maximum at 427 °C. The first weak, broad endothermic effect is irreversible, whereas the second, sharp endothermic peak is reversible. In contrast to ACF-013, the phase remaining after thermal analysis here was pure α-AlF_3. It is noteworthy that the exothermic peak at 427 °C is spread over a temperature interval of more than 200 °C, whereas for ACF-013 a very sharp effect was observed.

XRD and Catalysis. For a better understanding of the DTA curves obtained for ACF-013, the nature of the phases occurring during the heating of ACF was investigated by isochronous annealing of ACF-013 sealed in a quartz ampule for 20 min at temperatures of 300, 400, 500, and 600 °C, and recording the X-ray diffraction patterns[8] at room temperature. After annealing at 300 °C, the sample did not show any reflections. After annealing at 400 °C, intensive reflections of η-AlF_3 and weak ones of $AlCl_3$ occurred. After annealing at 500 °C, large reflections of θ-AlF_3 appeared together with a small ones of β-AlF_3; after annealing at 600 °C, β-AlF_3 was found along with a small amount of θ-AlF_3. At the latter two temperatures, $AlCl_3$ was not seen but could not be excluded, since its reflections overlap with either the β-AlF_3 or θ-AlF_3 ones.

Samples of ACF-013 annealed below 400 °C were as catalytically active as ACF-013. Samples annealed above 400 °C were inactive.

Evolution of Volatile Compounds. Since the sample for DTA analysis was sealed in an ampule, the evolved gases could not be analyzed simultaneously. Therefore, ACF-013 was heated with 10 K/min in flowing argon in a quartz reactor up to 600 °C, and the gas stream was analyzed by FTIR spectroscopy. It shows clearly that carbon containing species are evolved. Wavenumbers of the vibrations are given in parentheses.

Up to 250 °C, CCl_4 (795 cm^{-1}) is evolved with a maximum at 180 °C; $COCl_2$ (1830, 850 cm^{-1}) and HCl (2886 cm^{-1}) are released between 200 and 350 °C. A sudden sharp pulse of these gases and further of CO_2 (2350 cm^{-1}), CF_4 (1282 cm^{-1}), and SiF_4 (1032 cm^{-1}) is observed at the crystallization point. $COCl_2$, CO_2, HCl, and HF are produced during pyrohydrolysis of the sample. HF reacts with the quartz reactor and forms SiF_4.

4. Discussion

FTIR Spectra. All crystalline phases of AlF_3 known so far are built up of corner-sharing AlF_6 octahedra linked to a three-dimensional network ($_\infty{}^3[AlF_{6/2}]$).[26] The strong bands around 660 and 360 cm^{-1} in the crystalline phases (Figure 1) can be assigned to stretching and bending vibrations of

the corner-sharing AlF_6 octahedra. The Al−F bond lengths in both of these phases are almost equal.[27,28] So, the force constants of the vibrations and the reduced masses can expected to be almost equal. Therefore, the vibrational frequencies in both crystalline phases are very similar. An additional weak band originates from an Al−F−Al bending vibration.[29] Since the angles between the octahedra are different in both crystalline modifications, both bands have different frequencies.

In the case of ACF-013 and am-AlF_3, two strong bands are also observed at wavenumbers similar to those of α- and β-AlF_3 (Figure 1c,d). For these noncrystalline samples, the bands are significantly broader than those of the crystalline samples. The bands of ACF-013 are even broader than those of am-AlF_3. Therefore, it can be assumed that ACF-013 and am-AlF_3 are also built up of corner-sharing AlF_6 octahedra. The broader bands of ACF-013 indicate that the degree of disorder in this compound is higher than in am-AlF_3.

The main difference between the crystalline and the amorphous samples is that additional weak bands are not seen in the latter. This can be explained with the help of a simplified structure model for am-AlF_3 and ACF-013, in which the bond lengths, and especially the bond angles, are statistically distributed around a mean value. Bond lengths are usually very restricted, so their distribution is comparatively narrow. Since the distribution of the Al−F bond lengths causes a broadening of the bands of the AlF_6 stretching and bending vibrations, it does not shift the peak maxima significantly. Contrary to this, the Al−F−Al bond angle for corner-sharing octahedra can vary from about 132° to 180°.[30] Since the frequency of the Al−F−Al bending vibration strongly depends on this angle and there is no corresponding band visible in the IR spectrum, it can be concluded that these angles are distributed over a comparatively wide range. The bands of these bending vibrations become very broad and are completely superposed by the other two strong bands.

Cl K Edge XANES. The shape of the XANES spectrum of the Cl K edge in $AlCl_3$ changes significantly during fluorination with $CFCl_3$ (Figure 2). The resonance at 2826.0 eV develops during fluorination. These spectra can be regarded as a fingerprint for the local environment of chlorine. It is obvious that the electronic structures of the Cl atoms in $AlCl_3$ and ACF-013 are different from each other. Looking at the spectra of $AlCl_{2.39}F_{0.61}$ and $AlCl_{1.75}F_{1.25}$ (Figure 2), one can clearly see that these spectra are a superposition of the spectra of $AlCl_3$ and ACF-013. These compounds contain two different chlorine species: a species such as that in $AlCl_3$ and a species such as that in ACF-013.

^{19}F MAS NMR Experiments. The type 1 signals with δ_{iso} at around 0 ppm as in the AlF_3 phase correspond to ^{19}F nuclei shared by two AlF_6 octahedra (bridging fluorine). The contribution of type 2 signals with δ_{iso} around −40 ppm can be explained according to the so-called superposition model for the ^{19}F chemical shift.[31] This low value is consistent with F atoms with only one Al atom as the nearest neighbor (terminal or unshared fluorine) (Figure 5).

Hydrolysis results in the disappearance of the signals of the terminal ^{19}F atoms and a shift in the type 1 line to higher positive values. This shift is also observed going from water-free crystalline AlF_3 phases to the corresponding hydrates (Figure 6). Following that, it may be related to the presence of water molecules.

Furthermore, fluorine atoms shared between two AlF_6 octahedra that are responsible of the type 1 contribution could be classified in the following way: The contribution at $\delta_{iso} = -4.0$ ppm (around 25%, see Figure 5) may be related to fluorine atoms in a 3D almost regular AlF_6 octahedra network as in α-AlF_3, while the one at $\delta_{iso} = +3.5$ ppm (around 75%, see Figure 5) could be assigned to fluorine atoms in a more disordered network or at the surface.

From the ^{19}F measurements, except the lines related to the organic fluoride molecules, the main difference between ACF-013 and am-AlF_3 is the existence of these unusual low δ_{iso} values at about −40 ppm (compare Figure 6a,b). Thus, in ACF-013, it could be assumed that a small amount (4−5%) of unshared fluorides is present.

^{27}Al MAS SATRAS NMR Experiments. The simulation of the MAS SATRAS NMR spectra clearly shows that the distribution of quadrupolar frequencies is broader in ACF-013 than in am-AlF_3 (Figure 8). This is related to a larger disorder in the former phase. The 1D distribution functions $R(\nu Q) = \int_0^1 P_{d,\sigma}(\nu_Q, \eta_Q)\, d\eta_Q$ for both phases are given in Figure 9. The larger distribution width σ shows clearly that the degree of disorder in ACF-013 is higher than in am-AlF_3. The quadrupolar frequencies in the crystalline phases are not distributed but are fixed values (α-AlF_3, 35 ± 3 kHz; β-AlF_3, 120 ± 15 kHz[23,24]). For comparative purposes, they are also given with their error bars in Figure 9.

From the experiments on the partially fluorinated $AlCl_3$, it was demonstrated that an $AlCl_3$ crystalline phase coexists with a disordered ACF-013 phase. Linear regression of the $AlCl_3$ content versus the chlorine content x in $AlCl_xF_{3-x}$ (Figure 10) shows that for $x \leq 0.3$ the sample does not contain an $AlCl_3$ phase any more.

ESR Spectra. Fe^{3+} is easily and doubtlessly detected in aluminum chloride by its fine structure splitting (Figure 3a). Fe^{3+} substitutes for Al^{3+} on a regular lattice position. Starting from the corresponding single crystal data,[16] the simulation delivers a spectrum that acceptably agrees with the measured spectrum (Figure 3b).

Already in the first phase of the reaction with $CFCl_3$ at about 25 °C, the discrete Fe^{3+} spectrum disappears and changes into comparatively broad resonances in the $g' \sim 4.3$ and $g' \sim 2.0$ regions and at $g' \geq 2$ (Figure 3c). The simultaneous appearance of signals at $g' \sim 4.3$ and $g' \sim$

(26) Herron, N.; Thorn, D. L.; Harlow, R. L.; Jones, G. A.; Parise, J. B.; Fernandez-Baca, J. A.; Vogt, T. *Chem. Mater.* **1995**, *7*, 75−83.
(27) Daniel, P.; Bulou, A.; Rousseau, M.; Nouet, J.; Fourquet, J. L.; Leblanc, M.; Burriel, R. *J. Phys.: Condens. Matter* **1990**, *2*, 5663−5677.
(28) Le Bail, A.; Jacoboni, C.; Leblanc, M.; De Pape, R.; Duroy, H.; Fourquet, J. L. *J. Solid State Chem.* **1988**, *7*, 96−101.
(29) Bondam, J. *Acta Chem. Scand.* **1971**, *25*, 3271−3276.
(30) Müller, U. *Anorganische Strukturchemie*; Teubner-Verlag: Stuttgart, Germany, 1996; Chapter 15.
(31) Bureau, B.; Silly, G.; Buzaré, J. Y.; Emery, J. *Chem. Phys.* **1999**, *249*, 89−104.

2.0 is typical for Fe^{3+} in amorphous fluoride matrixes (Figure 3c,d).[11] From this, it can be concluded that some of the iron impurities at this temperature are incorporated into the arising amorphous ACF-013 phase. In addition, another part is forced to aggregate. Evidence for this is given by the very broad resonances at $g' \geq 2$: one in the region below 100 mT and another between 200 and 400 mT. Similar aggregation phenomena were also observed in fluoride glasses.[32]

As shown in Figure 4a,b, the spectra of ACF-013 are characterized by an intensive signal in the $g' \sim 2$ region. It has already been mentioned that these signals are essentially caused by chlorine-containing radicals, which are formed during the synthesis of ACF-013. At this point, the comparatively large thermal stability of such a radical is surprising. However, these observations are supported by the fact that a partially amorphous AlF_3 matrix is able to stabilize organic radicals and even atomic hydrogen up to the temperature region already mentioned.[33] Hence, the occurrence of the these radicals is further proof of the amorphicity of the ACF. The evolution of CCl_4 and $COCl_2$ during heating clearly shows that significant amounts of chlorine containing organic species are trapped in ACF-013. The radicals do not take part in the catalytic reaction used here.

The spectrum of the radical appears to be anisotropic, and at lower temperature, it is split into hyperfine components due to coupling with the chlorine nuclei ($I = {}^3/_2$ for ^{35}Cl and ^{37}Cl). Several of these hyperfine components are quite well resolved in the spectra of the samples with low fluorine content (Figure 4c), but only poorly resolved in ACF-013 (Figure 4a,b). This loss of spectral resolution gives direct evidence of the destruction of the crystalline structure during the synthesis of ACF-013. The samples of partially fluorinated $AlCl_3$ with a low fluorine content are mainly crystalline, which leads to comparatively sharp lines. The crystalline regions disappear, and the solid becomes amorphous with increasing amount of fluorine. This causes a statistical distribution of the spectral parameters, in this case the g-components ($\bar{g} = 2.017$) and the components of the hyperfine constants, and results in an effective line broadening in the spectrum.

Thermal Behavior. Heating up to about 350 °C does not change the bulk structure of ACF-013 significantly. The sample is still catalytically active and noncrystalline. At 400 °C, an irreversible, strongly exothermic phase separation takes place (Figure 11a). Crystalline AlF_3 and gaseous $AlCl_3$

$$AlCl_xF_{3-x} \rightarrow \frac{3-x}{3} AlF_3(cryst) + \frac{x}{3} AlCl_3(g)$$

are formed. After cooling, both solid phases are detected by X-ray diffraction. Further evidence for the formation of $AlCl_3$ is given by the observation of a reversible endothermic signal at 174 °C. It correlates very well with the sublimation temperature of $AlCl_3$ at 70 kPa.[34] It should be noted that the sublimation of $AlCl_3$ can only be observed when the sample was heated to a temperature above 400 °C at least once, and hence, $AlCl_3$ has been formed. This gives further proof that $AlCl_3$ does not exist as a separate phase in ACF-013.

The nature of the phase transition is evidenced by two more facts: (i) The catalytic activity of annealed samples of ACF-013 is high, as long as the annealing temperature is below 400 °C. (ii) Corresponding with the exothermic signal, a bunch of volatile organic compounds (mainly CCl_4, CF_4, and hydrolysis products) are evolved. So at this point, the structure completely decomposes and releases all the trapped species.

X-ray diffraction of ACF-013 annealed in an ampule up to the transition point of 400 °C shows η-AlF_3. At 500 °C, the main phase is θ-AlF_3; at 600 °C, it is β-AlF_3. This sequence is in good agreement with the DTA measurements, which show a weak, irreversible exothermic transition at 592 °C. Thus, this peak can be assigned to the reaction θ-$AlF_3 \rightarrow \beta$-AlF_3.

Up to now, all metastable phases of AlF_3 were reported to transform directly into α-AlF_3.[26] However, these phases seem to be relatively close to each other from a thermodynamic point of view. Slight changes in the reaction conditions (type and pressure of the gas phase) cause different phases to emerge. Surprisingly, this is the first time that a consecutive cascade of phase transformations is observed. In the closed ampules, certain partial pressures of $AlCl_3$ and AlF_3 develop on decomposition of ACF-013. Phase transitions as observed here seem to be very likely under conditions such as those used in our case, since, e.g., β-AlF_3 can be produced from α-AlF_3 in a chloride flux.[29]

The thermal behavior of am-AlF_3 strongly differs from that of ACF-013 (Figure 11b). As the first weak endothermic effect is irreversible, it is attributed to small amounts of water evolved by the solid that remained from the synthesis and could not be removed in a vacuum. The endothermic process occurring at about 250 °C seems to be closely related to the subsequent crystallization processes, the nature of which remains uncertain. It is noteworthy that the crystallization region is spread over a temperature interval of more than 200 °C and delivers α-AlF_3, whereas a very sharp effect is observed for ACF-013 and the product is β-AlF_3. Consequently, the crystallization process of ACF-013 is completely different from the one observed for am-AlF_3.

5. Conclusions

(i) The method published by DuPont for the synthesis of ACF seems to play a key role in obtaining unique properties of the resulting solid. Using low temperatures prevents the formation of ordered AlF_3 phases. Aluminum chloride and organic compounds present during synthesis further disturb the crystallization process. The latter can be detected in the ACF formed. In contrast to ACF, the am-AlF_3 phase does not exhibit strong Lewis acidity; it is inactive in the isomerization of 1,2-dibromohexafluoropropane.

(ii) Although ACF and am-AlF_3 are both X-ray amorphous materials mainly composed of aluminum and fluorine, their

(32) Scholz, G.; Stösser, R.; Grande, T.; Aasland, S. *Ber. Bunsen-Ges. Phys. Chem.* **1997**, *101*, 1291−1296.
(33) Scholz, G.; Stösser, R. *Phys. Chem. Chem. Phys.* **2002**, *4*, 5448−5457.
(34) *Gmelins Handbuch der Anorganischen Chemie, System-Nummer 35, Aluminium, Teil B*; Verlag Chemie GmbH: Germany, 1933; p 188.

local structures are different. ACF and am-AlF_3 are built up of corner-sharing AlF_6 octahedra. This is made clear by IR and NMR spectroscopy. These methods confirm a higher degree of disorder in ACF than in am-AlF_3. The X-band ESR spectra of both materials are also typical for disordered fluoride systems. ^{27}Al SATRAS NMR shows that ACF is the most distorted AlF_3 solid known so far. However, small amounts of nearly regular AlF_6 octahedra are present in the sample. Furthermore, terminal fluorine atoms, which are bound to only one aluminum atom, are evidenced by ^{19}F MAS NMR. They are a unique feature of the ACF phase. The fluorine atoms of am-AlF_3 bridge two AlF_6 octahedra; no terminal fluorine atoms exist.

(iii) Paramagnetic chlorine-containing species are trapped in cavities inside the amorphous ACF solid. These radicals are similar to those generated in CCl_4 by UV irradiation and are the subject of a separate study. The trapped radicals are stable up to 150 °C. They can be identified by their ESR spectra and do not change upon performance of heterogeneous catalytic reactions.

(iv) During heating, ACF forms crystalline metastable phases of AlF_3 and gaseous $AlCl_3$ at 401 °C. At crystallization, the volatile organic compounds trapped in cavities are released. The corresponding exothermic peak found by DTA is very sharp and narrow; crystallization takes place in a small temperature range of only 20 K. The thermal behavior of am-AlF_3 is completely different. Crystallization takes place over a range of more than 200 K. The peak in the DTA is broad resulting in the thermodynamically stable α-AlF_3 phase. Furthermore, an endothermic effect of unknown origin appears at around 250 °C.

(v) The high catalytic activity of ACF is related to the absence of a crystalline $AlCl_3$ phase. Residual chlorine in $AlCl_xF_{3-x}$ cannot be attributed to a separate, crystalline phase of $AlCl_3$, when $x \leq 0.3$. NMR, XANES, ESR, and DTA clearly prove this. This agrees with the values given by DuPont of $x = 0.05-0.3$ for the catalytically active ACF phase.

Acknowledgment. We would like to thank Dr. S. Schröder (Free University of Berlin) for the help in planning and performing the X-ray absorption measurements and Dr. A. Zehl (Humboldt University of Berlin) for ESR measurements.

IC034106H